# Sheffield Hallam University

# Elemental distributions within multiphase quaternary Pb chalcogenide thermoelectric materials determined through three-dimensional atom probe tomography

AMINORROAYA YAMINI, Sima <http://orcid.org/0000-0002-2312-8272>, LI, T., MITCHELL, D.R.G. and CAIRNEY, J.M.

## Published version

## Repository use policy

# Elemental distributions within multiphase quaternary Pb chalcogenide thermoelectric materials determined through three-dimensional atom probe tomography

**Sima Aminorroaya Yamini[1]\*, Tong Li[2], David R. G. Mitchell[1], Julie M. Cairney[2]\***

[1] *Australian Institute for Innovative Materials (AIIM), Innovation Campus, University of Wollongong, Squire Way, North Wollongong , NSW 2500 , Australia*
[2] *Australian Centre for Microscopy and Microanalysis, The University of Sydney, Madsen Building F09, NSW 2006, Camperdown, Australia*

*Corresponding authors: Sima Aminorroaya Yamini, Sima@uow.edu.au and Julie M. Cairney, Julie.Cairney@sydney.edu.au*

## Abstract

Nanostructured multiphase p-type lead chalcogenides have shown the highest efficiencies amongst thermoelectric materials. However, their electronic transport properties have been described assuming homogenous distribution of dopants between phases. Here, we have analyzed elemental distributions in precipitates and matrices of nanostructured multiphase quaternary Pb chalcogenides doped to levels below and above the solubility limit of the matrix, using three-dimensional atom probe tomography. We demonstrate that partitioning of sodium and selenium occur between the matrix and secondary phase in both lightly- and heavily-doped compounds and that the concentrations of sodium and selenium in precipitates are higher than those in the matrices. This can contribute to the transport properties of such multiphase compounds The sodium concentration reached ~3 at.% in sulfur-rich (PbS) precipitates and no nano precipitates of Na-rich phases were observed within either phase, a result that is supported by high resolution TEM analysis, indicating that the solubility limit of sodium in PbS is much higher than previously thought. However, non-equilibrium segregation of sodium is identified at the precipitates/matrix interfaces. These findings can lead to further advances in designing and characterizing multiphase thermoelectric materials.

**Keywords**: Thermoelectric materials, sodium, dopant, atom probe tomography, segregation, and solubility

## 1. Introduction

Bulk lead-chalcogenides provide the highest thermoelectric efficiencies amongst mid-range temperature (600-900 K) thermoelectric materials [1-5]. Intrinsic semiconducting lead chalcogenides can be tuned to either *n*-type or *p*-type to charge carrier concentrations of $10^{18}$ to $10^{19}$ cm$^{-3}$ due to excess lead or chalcogen atoms respectively, where point defects act as donor or

acceptor [6, 7]. However, some applications require carrier concentrations ranging from $\sim 10^{19}$ to $\sim 10^{21}$ cm$^{-3}$ [8, 9]. This is achieved by substituting some of the atoms with dopant elements of different valance [7]. Sodium is the most viable *p*-type dopant [1, 2, 10, 11] for Pb chalcogenides, though its solubility has been shown to be limited [12, 13]. Sodium doping results in considerably higher thermoelectric performance of *p*-type multiphase compounds when the alloys are doped at concentrations greater than the solubility limit of the matrix [2, 5, 11, 14]. We have attributed the high thermoelectric performance ($z$T $\sim$ 2) observed in heavily doped *p*-type quaternary Pb chalcogenides to heterogeneous distribution of sodium between the matrix and precipitates, with an enhanced contribution from modulation doping at elevated temperatures [5]. Dopant partitioning between PbTe-rich matrix and PbS-rich precipitates was identified in heavily-doped multiphase Pb-chalcogenides by energy dispersive X-ray spectroscopy analysis (EDS) in the transmission electron microscope (TEM) [5, 15, 16]. However, due to its limited sensitivity, this technique is unable to provide compositional information about dopant distribution in lightly-doped compounds. In the current study, we have employed three-dimensional (3D) atom-probe tomography (APT) to provide high sensitivity measurements of matrix and precipitate compositions, and to determine the spatial distribution of sodium both between and within individual phases in multiphase quaternary Pb chalcogenides at dopant concentrations below and above the solubility limit of the matrix.

We have explored a multi-phase nanostructured quaternary $(PbTe)_{0.65}(PbS)_{0.25}(PbSe)_{0.1}$ compound at sodium concentrations of 0.5 and 1.5 at.% ($Pb_{(1-x)}Na_xTe_{0.65}S_{0.25}Se_{0.1}$, $x$= 0.01, 0.03). Both compounds contain PbS-rich precipitates within a PbTe-rich matrix. The heavily-doped compound provides $z$T values of $\sim$2 at 800K and the lightly-doped compound delivers a maximum zT of $\sim$1 at 650 K. We demonstrate that partitioning of sodium occurs between the matrix and the secondary phase in both lightly- and heavily-doped materials, with higher sodium levels found in the sulfur-rich secondary phase. Selenium is also enriched in these precipitates relative to the matrix. Sodium is found to segregate strongly to the matrix/secondary phase interfaces. APT confirmed our high-resolution TEM analysis in that no nanoprecipitates of Na-rich phases were observed within phases.

## 2. Material and methods

*2.1. Sample Fabrication:* Polycrystalline samples of PbS and PbSe were prepared by mixing high purity Pb (99.999%), Se (99.999%), and dried S (99.9%) in vacuum-sealed quartz ampoules. These were reacted at 1373 K to produce high purity PbS and PbSe. The final polycrystalline $Pb_{(1-x)}Na_xTe_{0.65}S_{0.25}Se_{0.1}$ ($x$ = 0.01 and 0.03) samples were synthesized by mixing stoichiometric quantities of high purity PbS, PbSe, Pb, Te and Na. This mixture was sealed in carbon-coated

quartz tubes under vacuum and then reacted at 1373 K for 10 hours. The samples were quenched in cold water, followed by annealing at 823 K for 72 hours. The resulting ingots were hand-ground to powder in an agate mortar and pestle and sintered into 12 mm diameter disk-shaped pellets using spark plasma sintering (SPS) at 773 K and an axial pressure of 40 MPa for half an hour under vacuum.

***2.2. Thermoelectric properties measurements:*** Electrical conductivity and Seebeck coefficients were measured using a Linseis LSR-3 instrument. The thermal conductivity ($\kappa$) was calculated from $\kappa = \rho D_T C_p$. The laser flash method (Linseis LFA 1000) was used to measure the thermal diffusivity ($D_T$), the density ($\rho$) was calculated using the measured weight and dimensions. The specific heat capacity ($C_p$), was estimated by $C_p(k_B$ per atom$) = 3.07 + 4.7 \times 10^{-4} \times (T(/K) - 300)$ [17]. The Hall coefficient ($R_H$) was measured using the van de Pauw method [18].

***2.3. Materials characterization:*** The crystallographic structure of samples was characterized by X-ray diffraction (XRD) using a GBC Scientific X-Ray diffractometer with Cu K$_\alpha$ radiation ($\lambda$ = 1.544 Å, 40 kV, 30 mA). The sintered samples were characterized using a JEOL JEM-ARM200F aberration corrected scanning transmission electron microscope (STEM) operating at 200kV. TEM samples were prepared by cutting 3 mm diameter discs from wafers using a Leica TXP polisher, followed by grinding and polishing to 100 μm in thickness following by dimpling and Ar-ion milling to electron transparency using a Gatan PIPS.

***2.4. Atom Probe Tomography:*** The APT samples were prepared by the in-situ site-specific lift-out method [19] using focused ion beam (FIB) milling on a Zeiss Auriga instrument. The Mo TEM grid (Ted Pella) used as the substrate to hold the lift-out samples. The lift-out APT samples were sharpened to less than 100 nm in diameter at 5kV and 25 pA. The APT analyses were conducted using a local-electrode atom probe (LEAP) on a Cameca LEAP-4000X Si, equipped with a picosecond ultraviolet (UV) laser (wavelength = 355 nm) with a spot size of 2 μm. The detection efficiency is 50%. The APT experiment was carried out at 25 K, with a laser energy of 5 pJ, a pulse rate of 160 kHz and a target evaporation rate of 1 ion per 100 pulses. The APT data was analyzed using IVAS 3.6.6™ software. The point-by-point algorithm for characterization of the composition modulation operates in a virtual desktop run by Massive Launcher [20].

# 3. Results and discussion

**Figure 1(a)** shows the XRD patterns for both the lightly- and heavily-doped quaternary $(PbTe)_{0.65}(PbS)_{0.25}(PbSe)_{0.1}$ compounds. Alloying PbS with the single phase ternary system of $(PbTe)_{0.9}(PbSe)_{0.1}$, beyond its solubility limit results in the formation of PbS-rich precipitates within the PbTe-rich matrix with both phases exhibiting a NaCl-type face centred cubic (FCC)

crystal structure [21]. **Figure 1(a)** confirms the presence of both phases in the current study compounds. The room temperature carrier concentration of lightly- and heavily-doped samples are measured to be $3.8 \times 10^{19}$ cm$^{-3}$ and $1.3 \times 10^{20}$ cm$^{-3}$ respectively. The figure of merit of both samples as a function of temperature in the range of 300-850 K is shown in **Figure 1(b)**. The heavily-doped sample shows a much higher thermoelectric efficiency at temperatures above 600 K [5].
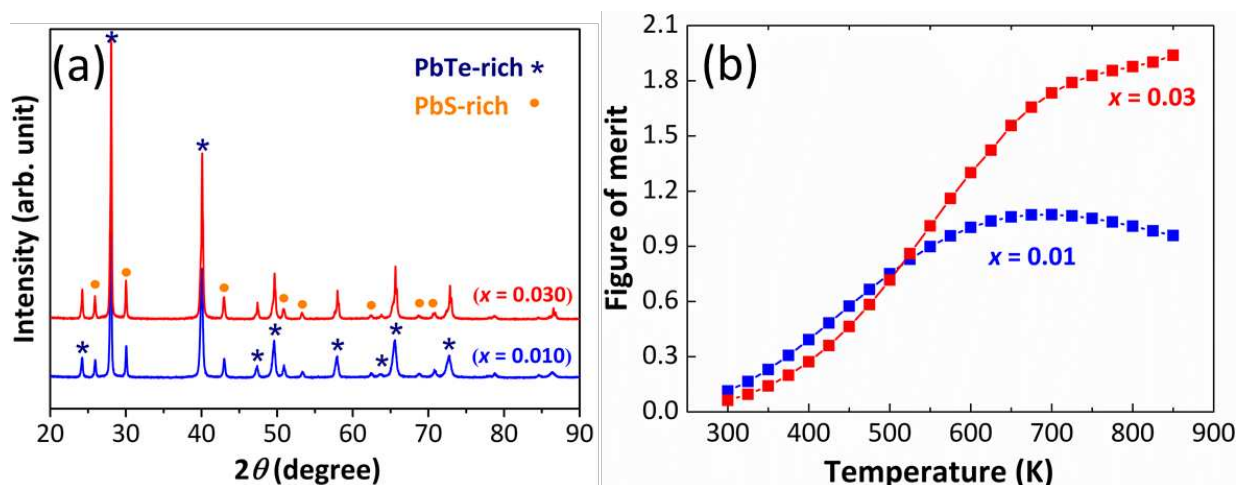


Figure 1. (a) Room temperature X-ray diffraction patterns and (b) figure of merit for $Pb_{(1-x)}Na_xTe_{0.65}S_{0.25}Se_{0.1}$ (x = 0.01, and 0.03) compounds.

## 3.1. Dopant partitioning and segregation

Five sets of atom probe data were acquired for each sample to obtain statistically valid information for both the PbS-rich precipitates and PbTe-rich matrix. Some atom probe specimens contained both phases while the others contained only the matrix or precipitate. **Figure 2 (a)** shows an example of a matrix (PbTe-rich)/precipitate (PbS-rich) interface in the lightly doped sample (x = 0.01). The sodium, sulfur, selenium and tellurium atom projections through a ~600 nm thick slice are shown, extracted from the total reconstructed volume of 100 million atoms. Detailed chemical analyses of the precipitate and matrix were performed using a proximity histogram, calculated based on an iso-concentration surface of 25.5% S (not shown). This iso-surface defines the precipitate-matrix interface, and the proximity histogram shows the average composition moving away from this surface (perpendicularly) throughout the dataset. The proximity histogram of sodium across at the precipitate/matrix interface (**Figure 2(b)**) shows a peak in sodium concentration (~ 1.2 at%) at the interface between the two phases. Away from the interfaces, the sodium concentration rapidly falls to much lower constant values of ~ 0.2 at.% in the matrix and ~0.6 at.% in the precipitate. This indicates that sodium partitioning to the

4

sulfur-rich precipitates occurs even in the samples with sodium concentrations below the solubility limit of the matrix (lightly-doped sample, $x = 0.01$).
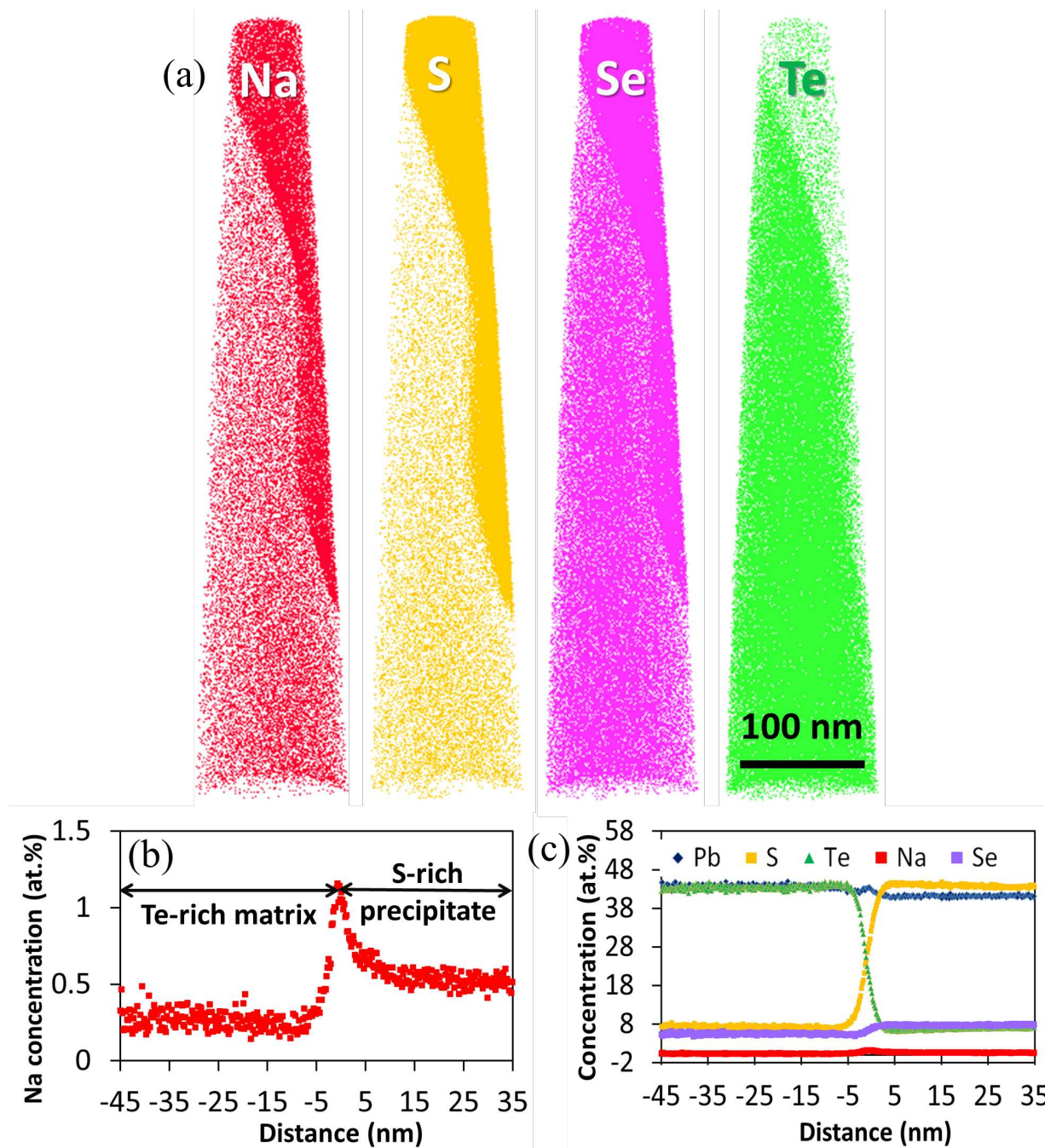


**Figure 2. Three-dimensional reconstruction of APT data for (a) sodium, sulfur, selenium and tellurium, (b) Proximity histogram showing the concentration profiles of Pb, Te, S, Se and Na across the interface of the two phases, (c) Proximity histogram displaying the concentration profiles of Na and Se for lightly doped $Pb_{0.99}Na_{0.01}Te_{0.65}S_{0.25}Se_{0.1}$ sample, showing higher concentration of sodium and selenium in the sulfur-rich precipitates.**

The interfacial concentration of sodium was 1.2 at.% and 4.5 at.% for the lightly- and heavily-doped samples respectively. Segregation of dopants to grain boundaries [22] and interfaces [2, 23] has been reported for thermoelectric materials often. Solute atoms in a crystalline structure segregate to grain boundaries, secondary phase interfaces and lattice imperfections including dislocations and stacking faults, in order to minimize the overall free energy of the system [24]. For both lightly- and heavily-doped samples, we have quantified the sodium segregation at the matrix/secondary interface by calculating the Gibbsian interfacial excess [25, 26]. We also analyzed the extent of segregation to the grain boundaries within the PbTe-rich matrix for the heavily doped sample (**see Supporting Information**). The compositions of two adjacent regions are assumed to be constant up to the interface that has no volume. Therefore, the excess atoms represent the excess number of solute atoms per unit area of the interface. This value is corrected for the detection efficiency (50%) because the calculation assumes an ideal detection efficiency for the single-ion detector [26]. The measured Na excesses at the interfaces for the various samples are shown in **Table I**.

**Table I. Interfacial excesses measured at the interfaces of PbTe-rich matrices and PbS-rich precipitates by atom-probe tomography**

| Nominal Na composition (at%) | Measured Na interfacial excess (nm$^{-2}$) | Measured Na excess at grain boundary of the matrix (nm$^{-2}$) |
|:---:|:---:|:---:|
| 0.5 | 2.08±0.13 | - |
| | 2.4±0.08 | |
| 1.5 | 10.55±0.2 | 1.75±0.06 |

There are large differences between the excess sodium measured at the interface of samples with different nominal Na concentrations and grain boundary. These significant excess sodium atoms suggest non-equilibrium segregation of sodium for these compounds. Equilibrium segregation is driven by lowering the interfacial free energy of the boundary when solute atoms are present. It is reversible and its magnitude decreases with increasing temperature. Non-equilibrium segregation of solute atoms is driven by the movement of vacancy atom complexes and/or dislocations to the interfaces and its extent increases with temperature due to an increase in the available vacancy concentration. The vacancies and dislocations are introduced to the solid by annealing at high temperatures, sintering or by deformation [27, 28]. Non-equilibrium segregation of sodium to PbS/PbTe interfaces has been also observed in a ternary PbTe-PbS system [23] and was correlated with fast cooling of the sample from the liquid state (over 3 hours). Isothermal annealing was recommended to attain equilibrium. Here, we observe non-equilibrium segregation of sodium in samples which have been annealed at 823K for three days [29]. Although homogenization of compounds with non-equilibrium segregation of solute atoms is possible by suitable aging, the usual fabrication methods for thermoelectric materials

(quenching, high temperature annealing and sintering) and the techniques used to measure the transport properties (continuous heating and cooling of samples) promote non-equilibrium segregation. Additionally, significant efforts have been made to introduce defects such as dislocations [30], grain boundaries [31] and precipitates [2, 32, 33] to thermoelectric materials to increase phonon scattering and consequently reduce the lattice thermal conductivity. Therefore, it is impossible to avoid non-equilibrium segregation in polycrystalline thermoelectric materials. Non-equilibrium segregation of sodium in multiphase Pb chalcogenides has attracted considerable attention due to the significant improvement achieved in thermoelectric performance of sodium-doped multiphase compounds at concentrations higher than the solubility limit of the matrix [2, 5, 11, 14, 33] and the low diffusion coefficient of Na in the PbTe matrix below 600 K [15, 34].

The excess sodium concentration measured at the interface of the matrix/precipitate is much higher than that at the grain boundary (**Table I**). Partitioning of Na between the matrix and precipitates for both lightly- and heavily-doped compounds is confirmed (**Figure 2(a)**) and it is known that partitioning of solute elements between the phases encourages the non-equilibrium segregation of solute atoms to interfaces [35]. Given that the magnitude of non-equilibrium segregation is known to increase with temperature [28], it seems reasonable to assume that this applies in the case of sodium. It would help explain the increase in Hall carrier concentration observed for the heavily-doped sample at temperatures above 600 K [5] **(See Supporting Information)**. A sudden increase in Hall carrier concentration as a function of temperature is the result of a combination of the thermodynamically driven process of sodium segregation to the interfaces and the kinetically driven diffusion-controlled migration of sodium atoms. The diffusion coefficient for sodium in PbTe indicates that it takes approximately two hours for sodium to diffuse 10 nm at 550K, whereas this time is reduced to 4 minutes at 600 K. The heating and cooling rates for the transport property measurements are much faster than the time required for samples to attain thermodynamic equilibrium at 550K and lower. However, it is possible for samples to reach equilibrium at temperatures at and above 600 K quickly. The observed jump at ~600K occurs due to rapid migration of sodium atoms with high thermodynamic driving force.

### 3.2. Dopant solubility

The nominal compositions of both lightly- and heavily-doped samples of $PbTe_{0.65}S_{0.25}Se_{0.1}$ and the average measured compositions of the sulfur–rich precipitates and the tellurium-rich matrix are summarised in **Tables II and III** respectively. The measured compositions are consistent with those expected for the solid solutions of PbTe-PbSe (matrix) and PbS-PbSe (precipitates) respectively. The proximity histogram across the precipitate/matrix interface for the lightly

doped sample (**Figure 2(c)**) indicates that the selenium concentration in the sulfur-rich precipitate is higher than that in the matrix. The atomic compositions of the phases presented in **Tables II and III** are obtained away from the interfaces to avoid variations caused by interfacial chemical inhomogeneity. The size of precipitates (>50 nm) was large enough to acquire accurate compositions >10 nm from the interfaces. The selenium concentration in precipitates is slightly higher than that of the matrices for both lightly- and heavily-doped compounds while the sulfur concentration ($\sim$ 3.7 at%) is the same in both. These selenium results are in agreement with the pseudo-ternary phase diagram of PbTe-PbSe-PbS [36], where it is shown that the selenium content in the PbS phase is higher than that in PbTe for the phase separated quaternary PbTe-PbSe-PbS systems. APT of a ternary PbTe-PbS system shows no tellurium in PbS precipitates [23] whereas, $\sim$2 at.% tellurium is detected in sulfur-rich precipitates of the quaternary system, indicating that selenium enhanced the tellurium solubility in sulfur-rich precipitates.

For the lightly-doped sample, the sodium concentrations are $\sim$0.60 at.% and $\sim$0.2 at.% in the precipitates and the matrix respectively. For the heavily-doped sample, these levels increased to 2.9 at.% and 0.6 at.% in the respective phases. The maximum solubility of sodium in PbTe is $\sim$0.7 at.% at 600K but this is reduced to 0.2 at.% at $\sim$ 500 K [12]. Alloying of PbTe with PbSe increases the sodium solubility limit in solid solution PbTe-PbSe systems [37]. PbS is shown to have a higher solubility for sodium compared with PbSe and PbTe [13]. The matrix of the current study compound contained $\sim$ 8 at.% PbSe and $\sim$7 at.% PbS. The sodium concentration of the matrix in a ternary PbTe-PbS system that contains $\sim$7 at.% PbS is measured to be 0.33 at.% [23]. This is lower than the 0.60 at.% detected in the quaternary system of the current study. The sodium content of precipitates reported for the ternary compound was $\sim$3.5 at.% which is much higher than the 2.8 at.% found in the current quaternary system. This is direct evidence that PbSe alloying increases the sodium solubility of the matrix compared to PbTe.

**Table II. The nominal composition and average measured composition of the matrix and precipitate for the lightly-doped sample of $Pb_{0.99}Na_{0.01}Te_{0.65}S_{0.25}Se_{0.1}$ analyzed by atom-probe tomography**

| Element | Nominal composition (at%) | Measured (at%) Matrix | Measured (at%) Precipitates |
|---------|---------------------------|------------------------|------------------------------|
| Pb | 49.5 | 45.9 ± 1.8 | 45.8 ± 2.1 |
| Te | 32.5 | 46.4 ± 2.5 | 2.1 ± 0.4 |
| S | 12.5 | 3.7 ± 0.8 | 44.4 ± 1.8 |
| Se | 5 | 3.7 ± 0.5 | 7.1 ± 0.8 |
| Na | 0.5 | 0.18 ± 0.02 | 0.6 ± 0.1 |

**Table III. The nominal composition and average measured composition of the matrix and precipitate for the heavily-doped sample of $Pb_{0.97}Na_{0.03}Te_{0.65}S_{0.25}Se_{0.1}$ analyzed by atom-probe tomography**

| Element | Nominal composition (at%) | Measured (at%) Matrix | Measured (at%) Precipitates |
|---------|---------------------------|------------------------|------------------------------|

| | | | |
|---|---|---|---|
| **Pb** | 48.5 | 51.4 ± 2.8 | 41.2 ± 0.3 |
| **Te** | 32.5 | 39.3 ± 3.5 | 3.3 ± 0.1 |
| **S** | 12.5 | 3.8 ± 0.6 | 45.7 ± 0.3 |
| **Se** | 5 | 4.7 ± 0.3 | 7.0 ± 0.1 |
| **Na** | 1.5 | 0.6 ± 0.2 | 2.9 ± 0.1 |

PbS precipitates in this study are alloyed with approximately 14 at.% PbSe. The latter has a lower solubility for sodium than PbS. The solubility of sodium in PbS is reported to be 2 at.% [13]. However, the first-principles density functional theory (DFT) calculations of Na-doped PbS suggests the existence of an as yet unknown ternary compound within the Na-Pb-S system [38]. The heavily-doped sample of the current study contains 2.9 at.% sodium, which is much higher than its reported solubility in PbS (2 at.%). We therefore used high-resolution TEM and carried out more detailed statistical analyses on the APT data to look for possible sodium-rich nanoprecipitates.

The bright field transmission electron microscopy (TEM) image of the heavily-doped sample (x = 0.03) in **Figure 3(a and b)** shows a dispersion of sulfur-rich precipitates. These images are taken with the electron beam parallel to the [001] and [111] axes. The [001] projection (**Figure 3(a)**) shows that the particles are roughly cuboidal, being bounded with {100}, {110} and {111} (based on Moiré contrast). Very strong Moiré fringes were present within the precipitates. These are caused by the overlap of precipitate and matrix lattices with different lattice spacings along the viewing direction. The similarity of the fringes within a grain indicates an orientation relationship between the two phases. Selected area electron diffraction (**Figures. 3(a) and (b) inset**) show the presence of weaker aligned reflections arising from the precipitate phase, confirming a cube//cube relationship. Weaker multiple reflections arise from double diffraction between the two phases.

The nature of the interface between the PbS precipitates and the PbTe matrix was also investigated with high resolution TEM (HRTEM) (**Figure 3(c)**). The image has been Fast Fourier Transform (average background subtraction (ABSF)) filtered to reduce noise and enhance the lattice contrast. The PbS precipitate shows periodic dark banding from the Moiré fringes evident within the precipitates in **Figures 3(a-b)**. The approximate position of the interface between the PbS and PbTe has been marked with aline. The dots indicate regions where the lattice planes are in phase. An edge dislocation in the PbS is marked with a 'T'. These accommodate the large (~ 7%) lattice mismatch strain between the two phases. No evidence was found for sodium-rich nanoprecipitates within either the matrix or the precipitate in our TEM analysis. Nanoprecipitates have been observed in Na-doped PbTe at concentrations above 0.5 at.% [13]. This confirms that the presence of selenium and sulfur in the quaternary Pb chalcogenides examined here increases the sodium solubility of the matrix.
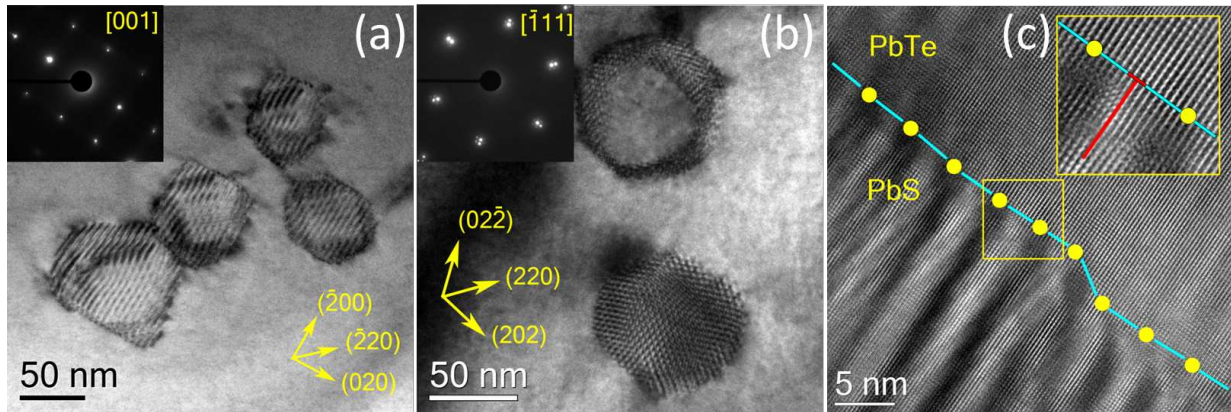
**Figure 3 TEM micrographs showing: (a) region tilted so that the beam is close to parallel with the [001] zone axis (inset SADP). The cuboidal 50-100nm PbS precipitates are mostly bounded by {100}, {110} and (from Moiré contrast) {111} planes; (b) a region tilted so that the beam is parallel to [111]. In both orientations aligned reflections indicate PbS//PbTe is in a cube//cube orientation. Strong Moiré fringes occur where the precipitate and matrix lattices overlap; (c) HRTEM image (ABSF filtered) of the boxed region in c) showing the interface between PbS and PbTe. The lattices are aligned, but edge dislocations (marked) occur in the PbS to accommodate the 7% lattice mismatch.**

To search for possible Na clustering in the Te-rich matrix and S-rich precipitate, a recently developed APT statistical test (a point-by-point analysis [20]) was used to analyze data from both lightly- and heavily-doped samples (**Figure 4**). This approach was chosen over conventional binomial analysis [39] due to improved sensitivity for nanoscale features with relatively minor deviations from randomized data [40]. A Z-test was further applied to measure the standard deviation of the frequency at a particular bin. In the Z-score test, values within ± 3 confirm that the hypothesis is correct, meaning that the experimental data is random with a 99% degree of confidence. In both the lightly- and heavily-doped samples (**Figure 4**), the Z-score tests indicate that the values are all within ± 3, suggesting that no Na clustering is present in either the Te-rich matrix or the S-rich precipitate, though it is partitioned between phases.
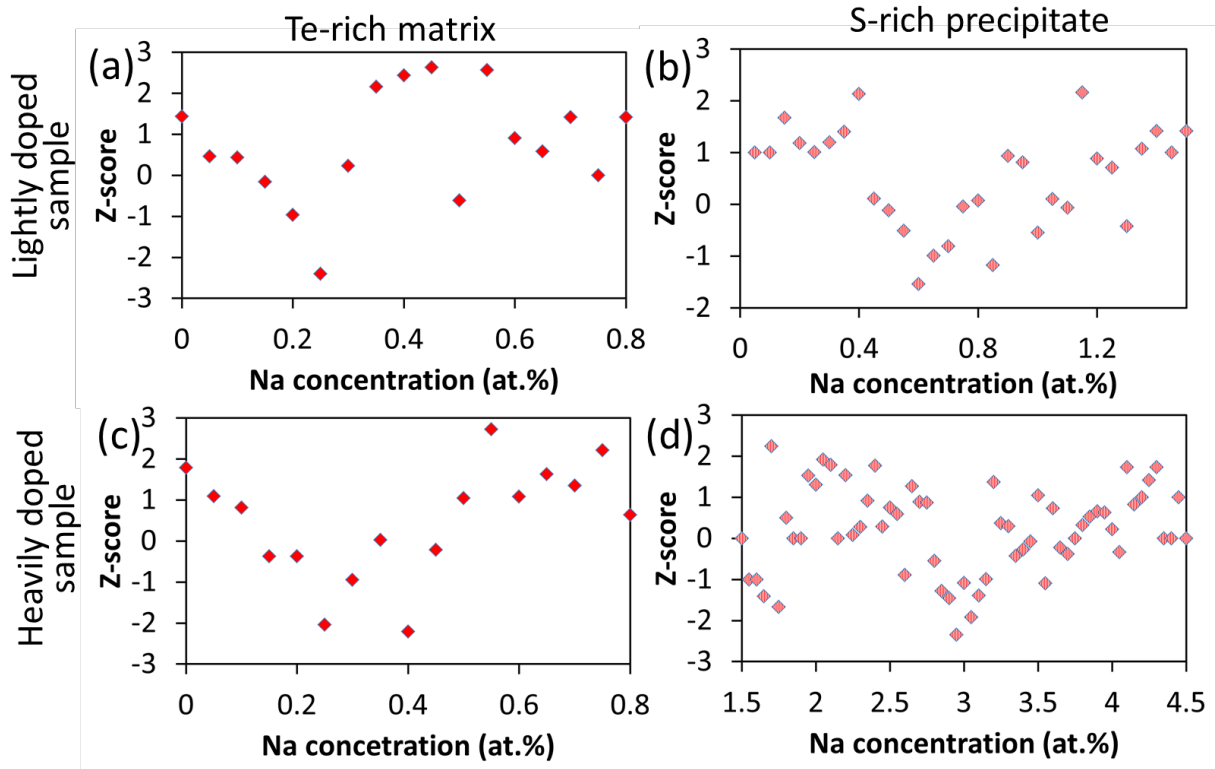
**Figure 4 Z-score test of point-by-point binomial analysis of atomic Na in (a) Te-rich matrix, (b) S-rich precipitate of the lightly-doped sample, and (c) Te-rich matrix and (d) S-rich precipitate of the heavily-doped sample.**

## 4. Conclusions

The outstanding thermoelectric performance of sodium-doped nanostructured multiphase Pb chalcogenides is achieved as a result of a heterogeneous distribution of dopants between matrices and secondary phases. APT was utilized to map the elemental distribution between precipitates and matrices of nanostructured multiphase quaternary Pb chalcogenides at dopant concentrations below and above the solubility limit of the matrix. We have shown that the sodium content in precipitates is much higher than that in matrices and that dopant partitioning occurs between phases for both lightly- and heavily-doped compounds. Precipitates also contain a higher concentration of Se than the matrices. Non-equilibrium segregation of sodium is identified at the matrix/precipitate interfaces. The sodium concentration in the PbS-rich secondary phase reached ~ 3 at.% without precipitation of Na-rich phases occurring, indicating sodium solubility in PbS is higher than previously thought (2 at%). Our detailed statistical analysis of APT data indicated complete solubility of sodium in the compounds with no Na-rich clusters identified. This was also supported by high-resolution TEM analysis. These results contribute to our understanding of the thermoelectric performance of multiphase compounds, providing useful information for designing thermoelectric materials with high efficiencies.

## 5. Acknowledgements

## 6. References

[1] Y. Pei, X. Shi, A. LaLonde, H. Wang, L. Chen, G.J. Snyder, Nature, 473 (2011) 66-69.
[2] K. Biswas, J. He, I.D. Blum, C.-I. Wu, T.P. Hogan, D.N. Seidman, V.P. Dravid, M.G. Kanatzidis, Nature, 489 (2012) 414-418.
[3] H. Liu, X. Shi, F. Xu, L. Zhang, W. Zhang, L. Chen, Q. Li, C. Uher, T. Day, G.J. Snyder, Nat Mater, 11 (2012) 422-425.
[4] Y. Gelbstein, J. Davidow, S.N. Girard, D.Y. Chung, M. Kanatzidis, Adv. Energy Mater., 3 (2013) 815-820.
[5] S. Aminorroaya Yamini, D.R.G. Mitchell, Z. Gibbs, R. Santos, V. Patterson, S. Li, Y.Z. Pei, S.X. Dou, G.J. Snyder, Adv. Energy Mater., 5 (2015) 1501047.
[6] R.F. Brebrick, E. Gubner, The Journal of Chemical Physics, 36 (1962) 1283-1289.
[7] Y.I. Ravich, B.A. Efimova, I.A. Smirnov, Semiconducting lead chalcogenides Plenum Press in New York1970.
[8] G.J. Snyder, E.S. Toberer, Nature Materials, 7 (2008) 105-114.
[9] L.E. Bell, Science, 321 (2008) 1457-1461.
[10] Y. Lee, S.-H. Lo, J. Androulakis, C.-I. Wu, L.-D. Zhao, D.-Y. Chung, T.P. Hogan, V.P. Dravid, M.G. Kanatzidis, J Am. Chem. Soc., 135 (2013) 5152-5160.
[11] L.-D. Zhao, J. He, C.-I. Wu, T.P. Hogan, X. Zhou, C. Uher, V.P. Dravid, M.G. Kanatzidis, J. Am. Chem. Soc., 134 (2012) 7902-7912.
[12] S. Aminorroaya Yamini, T. Ikeda, A. Lalonde, Y. Pei, S.X. Dou, G.J. Snyder, J. Mater. Chem. A, 1 (2013) 8725-8730.
[13] J. He, L.-D. Zhao, J.-C. Zheng, J.W. Doak, H. Wu, H.-Q. Wang, Y. Lee, C. Wolverton, M.G. Kanatzidis, V.P. Dravid, J. Am. Chem. Soc., 135 (2013) 4624-4627.
[14] L.-D. Zhao, S. Hao, S.-H. Lo, C.-I. Wu, X. Zhou, Y. Lee, H. Li, K. Biswas, T.P. Hogan, C. Uher, C. Wolverton, V.P. Dravid, M.G. Kanatzidis, J Am. Chem. Soc., 135 (2013) 7364-7370.
[15] S. Aminorroaya Yamini, David Mitchell, H. Wang, Z. Gibbs, Y. Pei, S.X. Dou, G.J. Snyder, AIP Advances, 5 (2014) 053601.
[16] J. He, J. Androulakis, M.G. Kanatzidis, V.P. Dravid, Nano Lett., 12 (2012) 343-347.
[17] A.S. Pashinkin, M.S. Mikhailova, A.S. Malkova, V.A. Fedorov, Inorg. Mater., 45 (2009) 1226-1229.
[18] K.A. Borup, E.S. Toberer, L.D. Zoltan, G. Nakatsukasa, M. Errico, J.-P. Fleurial, B.B. Iversen, G.J. Snyder, Rev. Sci. Instrum., 83 (2012) 123902-123907.
[19] K. Thompson, D. Lawrence, D.J. Larson, J.D. Olson, T.F. Kelly, B. Gorman, Ultmi, 107 (2007) 131-139.
[20] L.T. Stephenson, A.V. Ceguerra, T. Li, T. Rojhirunsakool, S. Nag, R. Banerjee, J.M. Cairney, S.P. Ringer, MethodsX, 1 (2014) 12-18.
[21] S. Aminorroaya Yamini, H. Wang, Z. Gibbs, Y. Pei, S.X. Dou, G.J. Snyder, Phys. Chem. Chem. Phys., 16 (2014) 1835-1840.
[22] Y. Tang, R. Hanus, S.-w. Chen, G.J. Snyder, Nat Commun, 6 (2015) 7584.
[23] Y.-J. Kim, I. Blum, J. He, M. Kanatzidis, V. Dravid, D. Seidman, JOM, 66 (2014) 2288-2297.
[24] P.J.E. Forsyth, R. King, G.J. Metcalfe, B. Chalmers, Nature, 158 (1946) 875-876.
[25] O.C. Hellman, D.N. Seidman, Materials Science and Engineering: A, 327 (2002) 24-28.
[26] M. Miller, Atom Probe Tomography: The Local Electrode Atom Probe, Springer2014.
[27] H.J. Grabke, H. Viefhaus, Surface segregation phenomena, in: P.A. Dowben, A. Miller (Eds.), CRC Press1990.
[28] D.R. Harries, A.D. Marwick, Philosophical Transactions of the Royal Society of London A: Mathematical, Physical and Engineering Sciences, 295 (1980) 197-207.

[29] S. Aminorroaya Yamini, M. Brewis, J. Byrnes, R. Santos, A. Manettas, Y.Z. Pei, Journal of Materials Chemistry C, 3 (2015) 10610-10615.

[30] S. Kim, K.H. Lee, H.A. Mun, H.S. Kim, S.W. Hwang, J.W. Roh, D.J. Yang, W.H. Shin, X.S. Li, Y.H. Lee, G.J. Snyder, S.W. Kim, Science, 348 (2015) 109-114.

[31] W. Liu, Z.F. Ren, G. Chen, Nanostructured thermoelectric materials, in: K. Koumoto, T. Mori (Eds.) Thermoelectric Nanomaterials, Springer Berlin Heidelberg2013, pp. 255-280.

[32] L.-D. Zhao, V.P. Dravid, M.G. Kanatzidis, Energy Environ. Sci., 7 (2014) 251-268.

[33] S. Aminorroaya Yamini, H. Wang, Z. Gibbs, Y. Pei, David Mitchell, S.X. Dou, G.J. Snyder, Acta Mater., 80 (2014) 365-372.

[34] A.J. Crocker, B.F. Dorning, J. Phys. Chem. Solids, 29 (1968) 155-161.

[35] G. Bruggeman, E.B. Kula, Segregation at interphase boundries, Syracuse University Press 1968.

[36] L. H, L.L.Y. Chang, MinM, 58 (1994) 567-578.

[37] I. Kudman, J. Mater. Sci., 7 (1972) 1027-1029.

[38] J.W. Doak, K.J. Michel, C. Wolverton, Journal of Materials Chemistry C, 3 (2015) 10630-10649.

[39] B. Gault, M.P. Moody, J.M. Cairney, S.P. Ringer, Atom probe microscopy, Springer-Verlag New York2012.

[40] L.T. Stephenson, M.P. Moody, P.V. Liddicoat, S.P. Ringer, Microscopy and Microanalysis, 13 (2007) 448-463.